Available online at www.sciencedirect.com
SCIENCE DIRECT®
Journal of Power Sources 149 (2005) 53–62
JOURNAL OF POWER SOURCES
www.elsevier.com/locate/jpowsour

Model-based prediction of suitable operating range of a SOFC for an Auxiliary Power Unit

Matthias Pfafferodt[a], Peter Heidebrecht[b], Michael Stelter[c], Kai Sundmacher[a,b,*]

[a] *Max Planck Institute (MPI), Dynamics of Complex Technical Systems, Sandtorstrasse 1, 39106 Magdeburg, Germany*
[b] *Process Systems Engineering, Otto-von-Guericke-University Magdeburg, Universitätsplatz 2, 39106 Magdeburg, Germany*
[c] *Webasto AG, Speicherstrasse 3-4, 17033 Neubrandenburg, Germany*

Received 31 August 2004; received in revised form 6 February 2005; accepted 7 February 2005
Available online 15 April 2005

Abstract

This paper presents a one-dimensional steady state model of a solid oxide fuel cell (SOFC) to be used in an Auxiliary Power Unit (APU). The fuel cell is fed a prereformed gas from an external autothermic reformer. In addition to the three electrochemical reactions (reduction of oxygen at the cathode, oxidation of hydrogen and carbon monoxide at the anode) the water–gas shift reaction and the methane steam reforming reaction are taken into account in the anode channel. The model predicts concentrations and temperatures and uses an equivalent circuit approach to describe the current–voltage characteristics of the cell. The model equations are presented and their implementation into the commercial mathematical software FEMLAB is discussed. An application of this model is used to determine suitable operating parameters with respect to optimum performance and allowable temperature.

Keywords: Solid oxide fuel cell (SOFC); Modelling and simulation; FEMLAB

1. Introduction

The fuel cell technology will be an important part of the future energy supply. Possible applications range from car engines to combined heat and power plants. Further on fuel cells can be used to provide electricity for mobile applications. Auxiliary Power Units (APU) are examples for such an application. An APU based on a solid oxide fuel cell (SOFC) is developed by the Webasto AG. It is supposed to supply trucks with electricity and it uses the available fuel – diesel or petrol. A hydrogen and carbon monoxide rich gas is produced in an external reformer and fed to the anode of the fuel cell. In contrary to gases normally used in solid oxide fuel cells this reformated gas contains less water and more than 50% nitrogen due to the air utilised in the reforming process. At the cathode pre-heated air is used.

The electrochemical reactions are described by an equivalent circuit diagram. The use of equivalent ohmic resistances for the mathematical description of the electrochemical reactions in a solid oxide fuel cell was first proposed by Achenbach [1]. This approach was used in several models to simulate the steady state performance of a SOFC [2–4]. Recently there are endeavours to simulate the dynamic behaviour using such an equivalent circuit diagram [5].

In this paper a model of a solid oxide fuel cell for an APU system is developed to predict suitable operating conditions. The specific composition of the anode gas as well as material specific limitations are considered. Further on it is shown how the operating point of the fuel cell can be optimised. For a fast and efficient simulation of the operating range a one-dimensional steady state model is sufficient. The simulations are done with the commercial mathematic software FEMLAB.

2. Modelling

The model presented here considers the smallest repeating unit of a co-flow or counter-flow solid oxide fuel cell stack.

* Corresponding author. Tel.: +49 391 611 0350; fax: +49 391 611 0353.
E-mail address: sundmacher@mpi-magdeburg.mpg.de (K. Sundmacher).

0378-7753/$ – see front matter © 2004 Elsevier B.V. All rights reserved.
doi:10.1016/j.jpowsour.2005.02.011

Nomenclature

Latin letters

c	concentration ($\mathrm{mol\,m^{-3}}$)
c_p	molar heat capacity ($\mathrm{J\,mol^{-1}\,K^{-1}}$)
E_A	activation energy ($\mathrm{J\,mol^{-1}}$)
F	Faraday's constant ($\mathrm{A\,s\,mol^{-1}}$)
g	molar flux density ($\mathrm{mol\,m^{-2}\,s^{-1}}$)
$\Delta_R g$	enthalpy of reaction ($\mathrm{J\,mol^{-1}}$)
h	height (m)
I	current (A)
i	current density ($\mathrm{A\,m^{-2}}$)
k	reaction rate constant ($\mathrm{mol\,m^{-3}}$)
K	equilibrium constant
n	number of transferred electrons
$\Delta_R h$	heat of reaction ($\mathrm{J\,mol^{-1}}$)
p	pressure (Pa)
q	heat flux density ($\mathrm{J\,m^{-2}\,s^{-1}}$)
R	gas constant ($\mathrm{J\,mol^{-1}\,K^{-1}}$)
$\tilde{R}$	area-related resistance ($\Omega\,\mathrm{m^2}$)
r	volumetric reaction rate ($\mathrm{mol\,m^{-3}}$)
T	temperature (K)
U	voltage (V)
U_{Nernst}	Nernst voltage (V)
u	velocity ($\mathrm{m\,s^{-1}}$)
x	molar fraction
z	coordinate (m)

Greek letters

α	heat-transfer coefficient ($\mathrm{W\,m^{-2}\,K^{-1}}$)
λ	heat conductivity ($\mathrm{W\,m^{-1}\,K^{-1}}$)
ν	stoichiometric coefficient

Subscripts

a	anode
avg	average
c	cathode
el	electric
eq	equilibrium
FC	fuel cell
i	index for the component
in	inlet
j	index for the reaction
pol	polarisation
ref	methane reforming
t	total
wgsr	water–gas shift reaction

Components

CH_4	methane
CO	carbon monoxide
CO_2	carbon dioxide
H_2	hydrogen
H_2O	water
N_2	nitrogen
O_2	oxygen

It consists of a single anode and cathode channel (Fig. 1). Thereby the complexity of the problem is reduced and the numerical computation time is short enough to perform repeated simulation in an acceptable time frame, making optimisation possible. Furthermore, the model complexity is reduced to only one spatial dimension by assuming plug flow in both channels, that is setting all gradients along the x- and y-coordinate to zero.

2.1. Model assumptions

The smallest repeating unit of a SOFC stack consists of three compartments: the cathode and the anode channel as well as the solid phase. The solid phase comprises all solid parts of the model (the bipolar plate, the cathode and anode electrode and the electrolyte). The structure of the model is shown in Fig. 2.

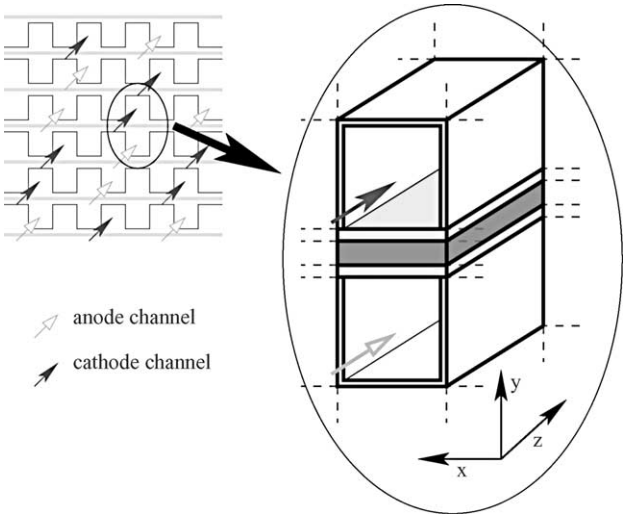

Fig. 1. Structural unit of a SOFC stack.

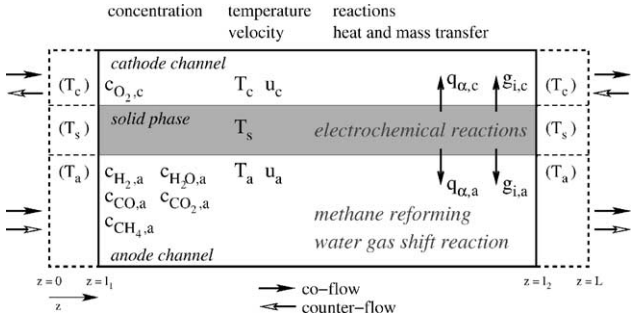

Fig. 2. Schematic one-dimensional representation of the SOFC model.

The temperature is calculated for each compartment of the model. Further on the velocity and the concentration of the components are considered for the cathode and the anode channel. The gas phases and the solid phase are interconnected via exchange of mass (molar flux density, g_i) and heat (heat flux density, q_α).

The electrochemical reactions take place inside the porous electrodes, which are considered to be a part of the solid phase. At the cathode oxygen is reduced

$$O_2 + 4\,e^- \rightarrow 2\,O^{2-} \tag{1}$$

whereas at the anode hydrogen and carbon monoxide are oxidised

$$H_2 + O^{2-} \rightarrow H_2O + 2\,e^- \tag{2}$$

$$CO + O^{2-} \rightarrow CO_2 + 2\,e^- \tag{3}$$

The reactions mentioned in Eqs. (1)–(3) result in the following two overall reactions:

$$H_2 + \tfrac{1}{2}O_2 + \rightarrow H_2O \tag{4}$$

$$CO + \tfrac{1}{2}\,O_2 + \rightarrow CO_2 \tag{5}$$

The fuel is converted to a hydrogen and carbon monoxide rich gas in an external reformer, which is not part of the model. The resulting gas contains a small amount of methane, which undergoes the strongly endothermic methane steam reforming reaction in the anode channel:

$$CH_4 + H_2O \leftrightharpoons CO + 3\,H_2 \tag{6}$$

Further on the slightly exothermic water–gas shift reaction is considered in the anode gas phase:

$$CO + H_2O \leftrightharpoons CO_2 + H_2 \tag{7}$$

Both reactions are included in the homogenous model of the gas in the anode channel.

Due to the design of the bipolar plate there is an inactive region before and after the active cell area (see Fig. 2). Within this region only the heat exchange between the anode gas, the solid and the cathode gas takes place. Neither the gas phase reactions in the anode channel nor the electrochemical reactions are considered here.

Further on the following assumptions are applied for the mathematical derivation of the model:

- Steady state operation is considered.
- The ideal gas law is applied for all gas components.
- The pressure in the model is considered as constant and equal to the standard pressure $p^\circ = 101.325\,\text{kPa}$. This condition is approximately fulfilled in the real world by the respective system design, which considers ambient pressure and low pressure drop along the channel.
- Plug-flow is assumed within the cathode and the anode channel. Thereby the gas temperature, the gas velocity and the composition only change along the z-coordinate.
- Only convective mass and heat transfer in z-direction are considered; diffusion and heat conduction phenomena are neglected in the gas phases. In the solid phase heat conduction along the spatial coordinate is considered.
- The methane steam reforming reaction and the water–gas shift reaction are considered as reversible, quasi-homogenous reactions which are at the chemical equilibrium. The enthalpy of this reactions is taken into account in the energy balance of the anode channel.
- The electrical conductivity of the bipolar plate is sufficiently high; therefore the ohmic resistance can be neglected. As a result the cell voltage is constant along the spatial cell coordinate.
- There are no concentration polarisations due to internal mass transport. In reality these effects are only observable at low concentrations of an educt component or at high current densities.

2.2. Model equations

Mass balances in both gas phases describe the composition and velocity in the anode and cathode channel. Enthalpy balances in temperature form yield the temperature in the gas phases and in the solid phase. Kinetic expressions are required for the heat exchange between the phases and for the reaction rates. The thermodynamic expressions from the National Institute of Science and Technology [6] are used to describe the temperature dependence of the gas properties. The coefficient equations for the heat capacity, the enthalpy and the Gibbs enthalpy are applied in the model.

2.2.1. Balance equations

The balance equations for both gas channels are similar. Therefore, only the equations for the anode channel are described below. The equations for the cathode channel can be obtained analogously. The only significant difference between them is that no gas phase reaction occurs in the cathode channel.

The differential equation for the concentration of the components in the gas phases is derived from the steady state continuous mass balance.

$$0 = -\frac{\partial}{\partial z}(c_{i,\text{a}}\,u_\text{a}) + \frac{g_{i,\text{a}}}{h_\text{a}} + \sum_j \nu_{i,j}\,r_j \tag{8}$$

Besides the convection term the mass transfer from and to the solid phase and the quasi-homogenous reactions in the gas phase are covered by this equation.

The following components i and reactions j are considered for the anode channel (index a):

$$i = H_2, CO, CO_2, CH_4, H_2O, \qquad j = \text{ref, wgsr}$$

For the cathode channel (index c) only the concentration of oxygen is calculated. There are no reactions in this channel.

$$i = O_2, \qquad j = \{\,\}$$

The concentration of nitrogen is obtained from the summation condition $c_t = \sum_i c_i$ using the ideal gas law $c_t = p/(RT)$ for the total concentration.

$$c_{N_2} = \frac{p}{RT} - \sum_{i \neq N_2} c_i \tag{9}$$

The differential equation for the velocity of the gas is derived from the overall mass balance:

$$0 = -\frac{\partial}{\partial z}(c_{t,a} u_a) + \sum_i \frac{g_{i,a}}{h_a} + \sum_j \overline{\nu}_j r_j \tag{10}$$

Insertion of the ideal gas law into Eq. (10) yields

$$0 = -\frac{p}{R}\frac{\partial}{\partial z}\left(\frac{1}{T_a} u_a\right) + \sum_i \frac{g_{i,a}}{h_a} + \sum_j \overline{\nu}_j r_j. \tag{11}$$

To solve Eq. (11) an additional differential equation for the temperature T_a must be given. The needed equation is obtained from the steady state enthalpy balance:

$$0 = -u_a c_{t,a} \overline{c_{p,a}} \frac{\partial T_a}{\partial z} + \sum_i c_{p,i} \frac{g_{i,a}}{h_a}(T_{a/s} - T_a) + \sum_j (-\Delta_R h_j) r_j + \frac{q_{\alpha,a}}{h_a} \tag{12}$$

with the average heat capacity $\overline{c_p} = \sum_i (c_{p,i} c_i / c_t)$.

The first term on the right hand side of Eq. (12) shows the convective enthalpy transport whereas the second term shows the temperature change as a result of the mass transfer between the solid phase and the gas phase. In Eq. (12), only the gas flow from the solid phase into the gas channel is taken into account (see Fig. 2) [7]:

$$T_{a/s} = \begin{cases} T_a, & \text{if } g_{i,a} < 0 \\ T_s, & \text{if } g_{i,a} > 0 \end{cases} \tag{13}$$

Further on, the reaction heat of the gas phase reactions in the anode channel and the heat transfer between the two compartments are included. A linear approach is used to describe the heat exchange:

$$q_{\alpha,a} = \alpha_a (T_s - T_a). \tag{14}$$

The value of the heat-transfer coefficient α_a is calculated for a reference velocity and composition in the anticipated temperature range [8]. A linear function is estimated from these values to describe the temperature dependence of the heat-transfer coefficient in the model.

A differential equation for the temperature of the solid phase can be obtained from the steady state enthalpy balance. Heat conduction according to Fourier's law, thermal drift due to mass transfer from and to the gas phase, convective heat exchange and a heat source due to the electrochemical reactions balance each other:

$$0 = h_s \lambda_s \frac{\partial^2 T_s}{\partial z^2} + \sum_i c_{p,i}\, g_{i,a}(T_{a/s} - T_s) + \sum_i c_{p,i}\, g_{i,c}(T_{c/s} - T_s) - q_{\alpha,a} - q_{\alpha,c} + q_s \tag{15}$$

Table 1
Boundary conditions applied to the differential Eqs. (8), (11), (12) and (15) for co-flow and counter-flow configuration

Left hand side ($z = 0$)	Variable	Right hand side ($z = L$)
Cathode channel (co-flow)		
$c_{O_2,c} = c_{O_2,c,in}$	$c_{O_2,c}$	$\frac{dc_{O_2,c}}{dz} = 0$
$u_c = u_{c,in}$	u_c	$\frac{du_c}{dz} = 0$
$T_c = T_{c,in}$	T_c	$\frac{dT_c}{dz} = 0$
Cathode channel (counter-flow)		
$\frac{dc_{O_2,c}}{dz} = 0$	$c_{O_2,c}$	$c_{O_2,c} = c_{O_2,c,in}$
$\frac{du_c}{dz} = 0$	u_c	$u_c = -u_{c,in}$
$\frac{dT_c}{dz} = 0$	T_c	$T_c = T_{c,in}$
Solid phase		
$\frac{dT_s}{dz} = 0$	T_s	$\frac{dT_s}{dz} = 0$
Anode channel		
$T_a = T_{a,in}$	T_a	$\frac{dT_a}{dz} = 0$
$u_a = u_{a,in}$	u_a	$\frac{du_a}{dz} = 0$
$c_{H_2,a} = c_{H_2,a,in}$	$c_{H_2,a}$	$\frac{dc_{H_2,a}}{difz} = 0$
$c_{CO,a} = c_{CO,a,in}$	$c_{CO,a}$	$\frac{dc_{CO,a}}{dz} = 0$
$c_{CO_2,a} = c_{CO_2,a,in}$	$c_{CO_2,a}$	$\frac{dc_{CO_2,a}}{dz} = 0$
$c_{H_2O,a} = c_{H_2O,a,in}$	$c_{H_2O,a}$	$\frac{dc_{H_2O,a}}{dz} = 0$
$c_{CH_4,a} = c_{CH_4,a,in}$	$c_{CH_4,a}$	$\frac{dc_{CH_4,a}}{dz} = 0$

FEMLAB requires two boundary conditions for each ODE.

The enthalpy of both overall reactions (see Eqs. (4) and (5)) are taken into account. A part of this energy is converted into electric power. The remaining energy is released as heat:

$$q_s = (-\Delta_R h_{el,H_2}) g_{H_2} + (-\Delta_R h_{el,CO}) g_{CO} - U_{FC}\, i_{el}. \tag{16}$$

In Eq. (16), $-\Delta_R h_{el,H_2}$ and $-\Delta_R h_{el,CO}$ characterise the reaction heat of the oxidation of hydrogen and carbon monoxide, respectively. g_{H_2} and g_{CO} describe the molar flux densities between the gas channel and the solid and can be considered as a representation of the reaction rate per unit electrolyt area.

For each of the presented differential equations, two boundary conditions are needed due to the fact that the simulation software FEMLAB uses parabolic differential equations of second order with respect to the spatial coordinate (Table 1). The inlet properties of the anode gas are assigned to the left hand side of the model ($z = 0$). According to the flow direction the inlet velocity, temperature and concentration for the cathode channel are specified at the left hand side (co-flow: $z = 0$) or at the right hand side (counter-flow: $z = L$). For the second boundary a zero gradient is assumed. Perfect insulation is assumed for both boundaries of the solid phase.

2.2.2. Kinetics of the anode gas phase reactions

In the anode channel of the model the methane steam reforming reaction and the water–gas shift reaction take place. Different expressions for the kinetics of both reactions can

be found in the literature (for example [2,3,9]). The kinetics depend on the exact composition of the electrode or catalyst material. They are not assignable to our simulations without great effort. Therefore, simple reaction mechanisms are used.

In this model chemical equilibrium of the gas phase reactions is assumed. According to Eq. (6), the equilibrium of the methane steam reforming reaction is given by

$$K_{\mathrm{ref,eq}} = \frac{x_{\mathrm{CO,a}}\, x_{\mathrm{H_2,a}}^3}{x_{\mathrm{CH_4,a}}\, x_{\mathrm{H_2O,a}}} \tag{17}$$

Analogously, the equilibrium of the water–gas shift reaction (Eq. (7)) can be written as:

$$K_{\mathrm{wgsr,eq}} = \frac{x_{\mathrm{CO_2,a}}\, x_{\mathrm{H_2,a}}}{x_{\mathrm{CO,a}}\, x_{\mathrm{H_2O,a}}} \tag{18}$$

with the molar fraction $x_i = c_i/c_\mathrm{t}$ and the equilibrium constant

$$K_{i,\mathrm{eq}} = \exp\left(\frac{-\Delta_\mathrm{R} g_i^\circ}{RT}\right) \tag{19}$$

where $\Delta_\mathrm{R} g_i^\circ$ is the standard Gibb's enthalpy of the reaction.

Eqs. (17) and (18) are algebraic equations, thus the resulting equation system is a differential algebraic system (DAE). The implementation of the equilibrium condition in algebraic form leads to unacceptable numerical complication. Therefore, we substitute these equations with finite reaction kinetics which fulfil the thermodynamic equilibrium conditions. To achieve gas compositions close to equilibrium at any point within the active cell area, the reaction rate constants are arbitrarily set to high values. Simple power-law reaction kinetics with an Arrhenius term are used for both reactions:

$$r_\mathrm{ref} = k_{\mathrm{ref},+,\infty} \exp\left(-\frac{E_\mathrm{A,ref}}{RT_\mathrm{a}}\right) \times \left[x_{\mathrm{CH_4,a}}\, x_{\mathrm{H_2O,a}} - \frac{x_{\mathrm{CO,a}}\, x_{\mathrm{H_2,a}}^3}{K_\mathrm{ref,eq}}\right] \tag{20}$$

$$r_\mathrm{wgsr} = k_{\mathrm{wgsr},+,\infty} \exp\left(-\frac{E_\mathrm{A,wgsr}}{RT_\mathrm{a}}\right) \times \left[x_{\mathrm{CO,a}}\, x_{\mathrm{H_2O,a}} - \frac{x_{\mathrm{CO_2,a}}\, x_{\mathrm{H_2,a}}}{K_\mathrm{wgsr,eq}}\right] \tag{21}$$

2.2.3. Electrochemical reactions

Two paths are considered for the electrochemical reactions. Either hydrogen or carbon monoxide can be electrochemically oxidised at the anode electrode. The kinetics of this reactions are described by using the approach of Achenbach [1]. Equivalent electric resistances are defined for the overpotentials at the cathode and at the anode. Furthermore, it is assumed that the resistance is independent of the local current density. The equivalent circuit diagram given in Fig. 3 illustrates this approach.

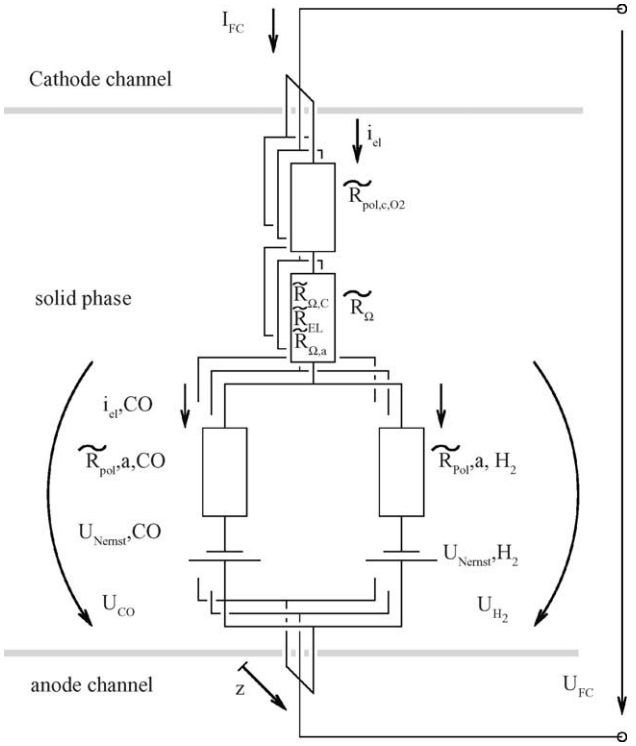

Fig. 3. Equivalent circuit diagram.

$$\tilde{R}_{\mathrm{pol,c,O_2}} = \left[\frac{4F}{RT} k_{\mathrm{O_2}} \left(x_{\mathrm{O_2,c}}\right)^{m_{\mathrm{O_2}}} \exp\left(-\frac{E_{\mathrm{A,pol,O_2}}}{RT_\mathrm{s}}\right)\right]^{-1} \tag{22}$$

$$\tilde{R}_{\mathrm{pol,a,H_2}} = \left[\frac{2F}{RT} k_{\mathrm{H_2}} \left(x_{\mathrm{H_2,a}}\right)^{m_{\mathrm{H_2}}} \exp\left(-\frac{E_{\mathrm{A,pol,H_2}}}{RT}\right)\right]^{-1} \tag{23}$$

$$\tilde{R}_{\mathrm{pol,a,CO}} = \left[\frac{2F}{RT} k_{\mathrm{CO}} \left(x_{\mathrm{CO,a}}\right)^{m_{\mathrm{CO}}} \exp\left(-\frac{E_{\mathrm{A,pol,CO}}}{RT}\right)\right]^{-1} \tag{24}$$

The constants used to calculate the polarisation resistances (Eqs. (22)–(24)) are listed in Table 2.

The total cell current I_FC is distributed along the z-coordinate as the local cell current density i_el, which is divided into $i_{\mathrm{el,H_2}}$ and $i_{\mathrm{el,CO}}$ according to the two parallel

Table 2
Constants used for the cathode and anode polarisation resistance [1]

	k (A/m^2)	$E_\mathrm{A,pol}$ (J/mol K)	m
$\tilde{R}_{\mathrm{pol,c,O_2}}$	14.9×10^9	160×10^3	0.25
$\tilde{R}_{\mathrm{pol,a,H_2}}$	0.213×10^9	110×10^3	0.25
$\tilde{R}_{\mathrm{pol,a,CO}}$	0.298×10^9	110×10^3	0.25

reaction paths:

$$I_{FC} = \int_{z=l_2}^{z=l_1} i_{el} b \, dz = \int_{z=l_2}^{z=l_1} \left(i_{el,H_2} + i_{el,CO}\right) b \, dz = i_{avg} A_{cell} \quad (25)$$

with i_{avg} as the average current density and A_{cell} as the active cell area. The electric resistances $\tilde{R}$ and the Nernst voltages U_{Nernst} are also local values whereas the cell voltage U_{FC} is constant along the channel.

A mathematical description of the equivalent circuit diagram is obtained from Kirchhoff's laws:

$$i_{el} = i_{el,H_2} + i_{el,CO} \quad (26)$$

$$U_{H_2} = U_{CO} \quad (27)$$

$$U_{H_2} = U_{Nernst,H_2} - i_{el,H_2} \cdot \tilde{R}_{pol,a,H_2} \quad (28)$$

$$U_{CO} = U_{Nernst,CO} - i_{el,CO} \cdot \tilde{R}_{pol,a,CO} \quad (29)$$

$$U_{FC} = U_{H_2} - (\tilde{R}_{pol,c} + \tilde{R}_{\Omega}) i_{el} \quad (30)$$

$$\tilde{R}_{\Omega} = \tilde{R}_{\Omega,c} + \tilde{R}_{el} + \tilde{R}_{\Omega,a} \quad (31)$$

whereas the ohmic resistance of the anode electrode ($\tilde{R}_{\Omega,a}$) and the cathode electrode ($\tilde{R}_{\Omega,c}$) as well as the resistance for the oxygen ions in the electrolyte (R_{el}) are calculated using the equations given by Achenbach [1].

The Nernst voltage required in the Eqs. (28) and (29) is given by:

$$U_{Nernst,H_2} = \frac{-\Delta_R g^{\circ}{}_{H_2}}{2F} + \frac{RT}{2F} \ln\left(\frac{\sqrt{x_{O_2,c}} x_{H_2,a}}{x_{H_2O,a}}\right) \quad (32)$$

and

$$U_{Nernst,CO} = \frac{-\Delta_R g^{\circ}{}_{CO}}{2F} + \frac{RT}{2F} \ln\left(\frac{\sqrt{x_{O_2,c}} x_{CO,a}}{x_{CO_2,a}}\right). \quad (33)$$

The connection between the current density and the molar flux density is given by Faraday's law. It is applied for the oxidation of hydrogen and the oxidation of carbon monoxide at the anode and analogously for the reduction of oxygen at the cathode.

$$i_{el,H_2} = n_{H_2} g_{H_2,a} F \quad (34)$$

$$i_{el,CO} = n_{CO} g_{CO,a} F \quad (35)$$

$$i_{el} = n_{O_2} g_{O_2,c} F \quad (36)$$

In the equations above n is the number of transferred electrons in the reduction and oxidation process, respectively. The molar flux density of the mass exchange flux between the gas channel and the solid phase is represented by g (see Fig. 2). F stands for Faraday's constant.

2.3. Definition of the operating point

An additional input parameter is required to define the operating point in the current–voltage plain of the fuel cell. On the one hand it is possible to specify a certain cell voltage (potentiostatic mode), on the other hand the cell current can be given (galvanostatic mode).

For the potentiostatic mode the cell current is easily calculated from the charge balance as the integral of the current density over the active cell area (Eq. (25)). An integral condition has to be solved for the galvanostatic mode:

$$F_I(U_{FC}) = I_{FC} - I^*(U_{FC}) \overset{!}{\Rightarrow} 0 \quad (37)$$

where I_{FC} is the given cell current and I^* is defined as

$$I^* = \int_{z=l_2}^{z=l_1} i_{el}(U_{FC}, x_{i,a}(z), x_{i,c}(z), T_S(z)) b \, dz \quad (38)$$

This means that U_{FC} has to be varied in such a manner that Eq. (37) is fulfilled.

3. Implementation in FEMLAB

The commercial modelling environment FEMLAB 2.3 is used to solve the set of governing equations. The program provides a number of predefined partial differential equations (PDEs) from several areas of science and engineering (referred to as application modes). Additional model specific PDEs can be defined. All equations are solved simultaneously by applying the finite element method (FEM). A specific documentation of all abilities of FEMLAB can be found in the manuals [10,11].

A one-dimensional geometry consisting of three subdomains is created by using the graphical user interface (GUI). The middle subdomain is the active cell area with inactive regions on the left and on the right.

The model uses differential equations to calculate the composition and velocity of the gas in both channels as well as the temperature in all three compartments. A *convection and diffusion* application mode is used for the partial mass balance in the gas phases (Eq. (8)) whereas the temperatures in the gas channels (Eq. (12)) are described in a *convection and conduction* mode. In the solid phase the enthalpy balance (Eq. (15)) is implemented in a *heat transfer* application mode. Given that the equation used for the velocity (Eq. (11)) does not exist as a predefined application mode, a *pde general form* is applied. The boundary conditions for all equations are listed in Table 1.

The integral condition (Eqs. (37) and (38)) to set the cell current in the galvanostatic mode is implemented using a *weak boundary* and a *weak subdomain* application mode. Due to this, the weak form of the PDEs has to be used to solve the problem.

Furthermore, all equations regarding the calculation of interim values are supplied as expressions. Parameters and other constant values are entered as constants.

The results are calculated using the stationary non-linear solver. Due to the strong non-linearity of the problem, it is

Table 3
Definition of the reference case

Description	Variable	Value
Electrical characteristics		
Current (A)	I_{FC}	0.45
Gas properties at the cathode inlet		
Temperature (K)	$T_{c,in}$	923
Velocity ($m\,s^{-1}$)	$u_{c,in}$	0.4
Compound		
Oxygen	$x_{O_2,c,in}$	0.21
Nitrogen	$x_{N_2,c,in}$	0.79
Gas properties at the anode inlet		
Temperature (K)	$T_{a,in}$	1123
Velocity ($m\,s^{-1}$)	$u_{a,in}$	0.5
Compound		
Hydrogen	$x_{H_2,a,in}$	0.22
Carbon monoxide	$x_{CO,a,in}$	0.20
Carbon dioxide	$x_{CO_2,a,in}$	0.02
Water	$x_{H_2O,a,in}$	0.03
Methane	$x_{CH_4,a,in}$	0.001
Nitrogen	$x_{N_2,a,in}$	0.529

hard to find an initial guess such that the solution converges. Therefore the parametric solver is applied. First, the steady state is calculated with a current of $I_{FC} = 0.01$ A as a parameter. Then, the cell current is increased stepwise. For each new value the solution of the old parameter is used as an initial guess. The result is the current voltage characteristic of the cell.

4. Results

The model is used to estimate the steady state of the SOFC stack. Calculations are done for the co-flow and the counter-flow configuration and a first analysis of the operating range is performed.

4.1. Operation conditions at reference case

The values used in the reference case are shown in Table 3. The galvanostatic operation mode is applied for the simulations. The current of $I_{FC} = 0.45$ A is equivalent to an average current density of $i_{avg} = 250\,mA/cm^2$.

At the cathode inlet pre-heated air at a temperature of 923 K enters the fuel cell whereas at the anode inlet gas from the external reformer is used. The composition approximates the equilibrium molar fractions after the partial oxidation of diesel at 1123 K with an air to fuel ratio of 0.4.

4.2. Co-flow

The flow direction in the cathode and the anode channel are identical in the co-flow case. The temperature distribution in both channels and in the solid phase is shown in Fig. 4. Within the inactive regions, the temperatures of the cathode air and the anode gas approach the solid temperature. It results in an average temperature of approximately 1035 K at the boundary between the inactive region and the active area. After that the temperature increases as a result of the heat which is released by the electrochemical reaction. Since the solid phase is heated by the electrochemical reaction, its temperature is highest, while the temperatures of the cathode air and the anode gas are up to 10 K lower. A temperature of approximately 1210 K is reached at the end of the active cell area.

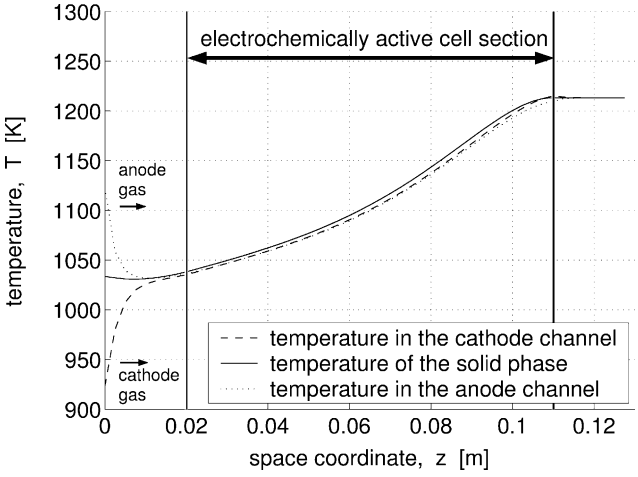

Fig. 4. Temperature distribution (co-flow) at reference conditions.

Fig. 5 shows the corresponding current density. The graph follows the temperature distribution in the active cell area. The electric resistance decreases with increasing temperature. Due to Ohm's law and the constant cell voltage, the current density rises accordingly.

The composition of the gas mixture in the cathode channel is shown in Fig. 6. The consumption rate of oxygen increases with rising current density. Therefore, the concentration of O_2 in the cathode channel decreases accordingly. Under the conditions defined in the reference case, the molar fraction of oxygen in the gas decreases from 21 to 16.5%. The curve

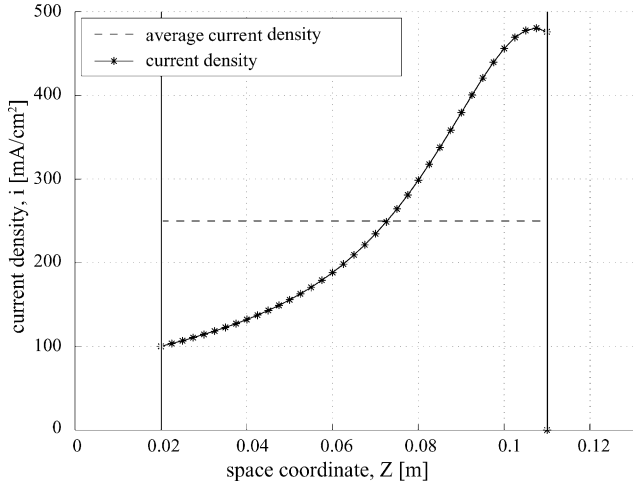

Fig. 5. Current density distribution (co-flow) at reference conditions.

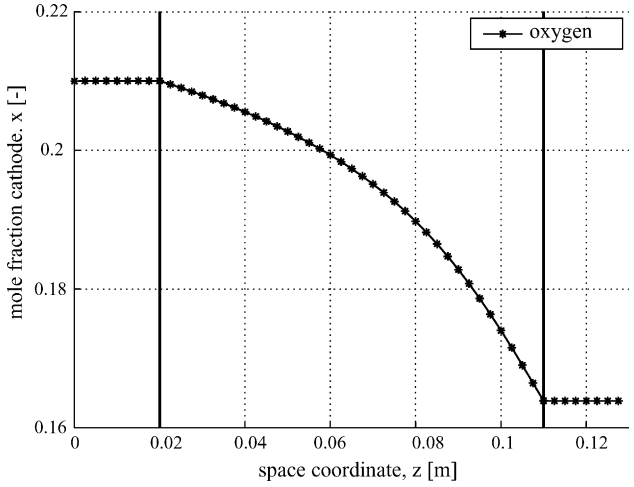

Fig. 6. Composition of the cathode gas (co-flow) at reference conditions.

corresponds to the temperature and current density distribution.

In addition to the electrochemical reactions the water–gas shift reaction and the methane steam reforming reaction are regarded in the anode channel (Fig. 7).

The concentration of hydrogen is almost constant in the first part of the active cell area. The hydrogen oxidised by the electrochemical reaction is balanced by the water–gas shift reaction. Since the anode gas is cooled down within the inactive region, the water–gas shift reaction is no longer at the chemical equilibrium. Thus carbon monoxide reacts with water to carbon dioxide and hydrogen. The change of the composition by the progressive oxidation of H_2 and CO as well as the increase of the temperature leads to a crossing of the equilibrium of the water–gas shift reaction. Afterwards the reverse water gas shift reaction outbalances this reaction. An indicator is the increasing water concentration and the relatively stable molar fraction of carbon monoxide in the second half part of the active cell area.

Table 4
Simulation results for the reference case (co-flow)

Simulated state	Variable	Value
Average current density (mA cm^2)	$i_{\mathrm{el,avg}}$	250.0
Voltage (V)	U_{FC}	0.67
Average power density (mW cm^2)	$p_{\mathrm{el,avg}}$	167.5
Average solid temperature (K)	$T_{\mathrm{s,avg}}$	1116
Maximum solid temperature (K)	$T_{\mathrm{s,max}}$	1213

A summary of characteristic process values for the co-flow operating mode can be found in Table 4.

4.3. Counter-flow

The cathode air inlet and fuel inlet are on opposite sides for the counter-flow case. The resulting temperature distribution is displayed in Fig. 8.

The gases at the outlets are cooled down by the gas at the corresponding inlet. The heat produced by the electrochemical reaction can not be discharged and the temperature adjusts to the displayed distribution for the steady state. The maximum temperature $T_{\mathrm{s,max}} \approx 1400$ K can be found in the middle of the active cell area.

The maximum temperatures are very high compared to the co-flow case. Accordingly this results in a higher temperature stress in the materials. Due to the allowed maximal temperature of 1250 K the counter-flow mode is not recommended for SOFC operating and is therefore not considered for the following analyses [5].

4.4. Isothermal U–I characteristics

The operational behaviour of the solid oxide fuel cell stack is described by its current–voltage characteristics. The computation of these characteristics can be done on the one hand by the specification of the cell voltage (potentiostatic) or on the other hand by the specification of the cell current (gal-

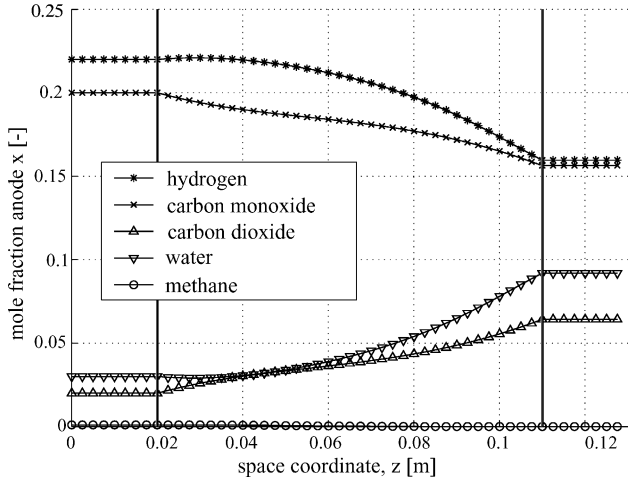

Fig. 7. Composition of the anode gas (co-flow) at reference conditions.

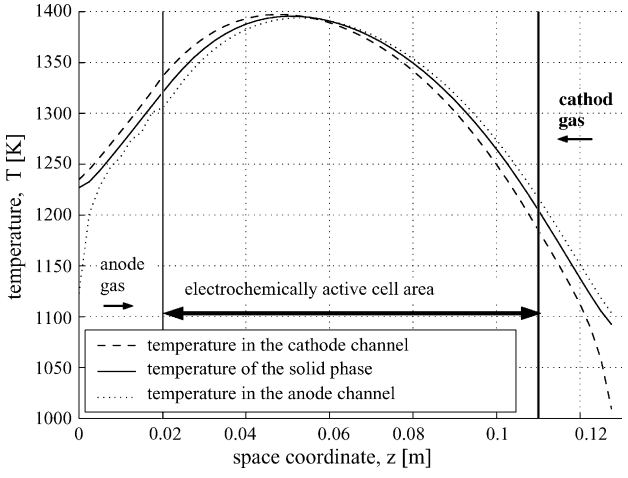

Fig. 8. Temperature distribution (counter-flow) at reference conditions.

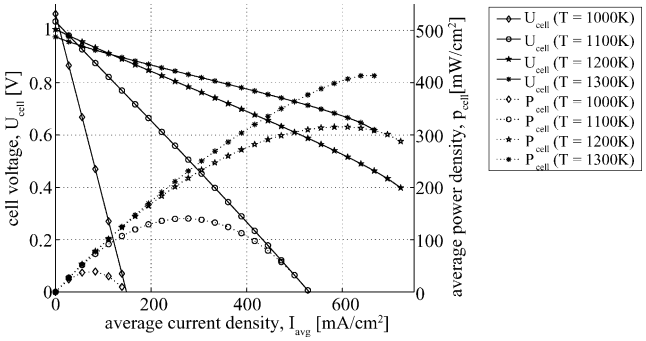

Fig. 9. Isotherm *U–I* characteristic.

vanostatic). Both variants result in the same current–voltage characteristics.

The current–voltage characteristic of a solid oxide fuel cell is measured at constant cell temperature. To make these simulations comparable to these experiments, isothermal conditions are used. Fig. 9 shows the *U–I* characteristic for a constant cell temperature of 1000, 1100, 1200 and 1300 K. The galvanostatic mode is used to calculate the curves.

The electric resistance only depends on the temperature and the concentration of the educt gases. As an isothermal model is considered and the influence of the educt concentration shows only at high current densities, the voltage loss rises linearly according to Ohm's law. Furthermore the difference between the curves diminishes with increasing temperature and the maximum of the power density shifts to higher current densities.

Fig. 10 shows the voltage losses caused by each electrical and electrochemical element at a temperate of 1200 K. The losses due to the polarisation resistance at the cathode and the ion transport through the electrolyte are of similar order of magnitude. At the anode the oxidation of hydrogen and the oxidation of carbon monoxide have to be considered together. The overall voltage loss at the anode can be estimated with a parallel connection of the corresponding polarisation resistances. This results in a voltage loss of about $\frac{1}{3}$ of the cathodic loss. The effect of the ohmic resistances of the cathode and the anode material on the cell voltage can be neglected.

Further investigation of the polarisation resistances as well as an analysis of sensitivity to the thickness of the individual cell components are done by Chen et al. [12]. They compare activation and concentration polarisation for electrolyte supported and anode supported cells. The results for electrolyte supported cells correspond qualitatively to the results shown in Fig. 10.

4.5. Operating range

The solid oxide fuel cell used for the APU system represents a complex chemical and physical system. Due to the material stresses there are limitations to the operating range, i.e. there are restrictions for the system variables. The relevant variables are the concentrations, the velocities, the current density and the temperature distributions.

The presented simulation describes the steady state of the solid oxide fuel cell. The steady state of the system depends on the value of the input parameters, which can be divided into three groups according to their impact:

- The fuel at the anode inlet:

  The temperature ($T_{\mathrm{a,in}}$), the velocity ($u_{\mathrm{a,in}}$) as well as the composition of the anode gas ($x_{i,\mathrm{a,in}}$) have to be defined for the simulation. The needed hydrogen and carbon monoxide rich gas is produced by the partial oxidation of diesel in the reformer. For the simulation it is assumed that the external reformer is operated at an optimal operating point. Therefore the composition, velocity and temperature of the anode gas is considered to be constant.
- The air at the cathode inlet:

  For the cathode air the composition at the inlet is considered to be constant (79% N_2 and 21% O_2). But the inlet temperature ($T_{\mathrm{c,in}}$) as well as the inlet velocity ($u_{\mathrm{c,in}}$) can be varied. The temperature distribution is significantly affected by both values. With an increasing velocity or a decreasing temperature at the air inlet the fuel cell is cooled more intensively. As a result the polarisation resistances and thus the voltage losses rise.

  In contrast to the characteristics of the fuel the parameters at the cathode inlet can be changed relatively easily. The velocity is specified by the blower, whereas the temperature is determined by a heat exchanger.
- Electrical input parameter:

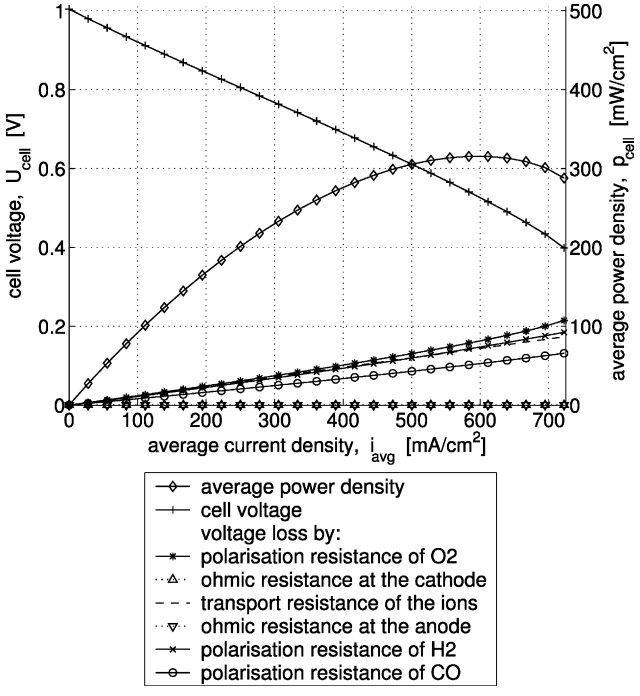

Fig. 10. Resistance.

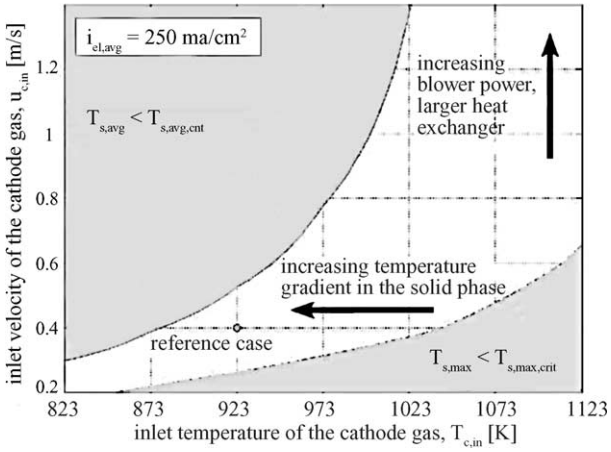

Fig. 11. Operating range for an average current density of $i_{el,avg} = 250.0\,mA\,cm^2$.

For the definition of an operating point either the cell current (galvanostatic) or the cell voltage (potentiostatic) must be given.

The possible operating range is limited by material properties, especially the maximum thermal stress. For this simulation a maximum temperature in the solid of $T_{s,max,crit} = 1250\,K$ is considered. Furthermore the average solid temperature should not drop below $T_{s,avg,crit} = 1100\,K$ or the cell voltage decrease to a point where the nickel catalyst, which is used in the anode electrode, starts to react electrochemically. At a temperature of $T_s = 1123\,K$ a critical cell voltage of $U_{FC} = 0.6\,V$ should be considered.

In Fig. 11, the operating range is displayed for a current density of $i_{el,avg} = 250.0\,mA\,cm^2$ depending on the cathode inlet velocity and temperature. The boundaries of the admissible operating range given by the average and maximum solid temperature are also drawn.

Further restrictions for the operating range are the maximum temperature gradient in the solid as well as the maximum blower power and the size of the heat exchanger. Similar analysis can be carried out for other current densities and thereby an optimal operation point can be determined within the resulting three dimensional space at which a maximum power density is attained.

5. Conclusions

A one-dimensional stationary model of a SOFC used in an Auxiliary Power Unit has been presented. At the cathode of the fuel cell the reduction of oxygen is considered, while at the anode both the oxidation of hydrogen and the oxidation of carbon monoxide are regarded. For the polarisation resistances the approach of Achenbach [1] is used. The modelling covers the water–gas shift reaction as well as the methane steam reforming reaction in the anode channel of the fuel cell.

The commercial mathematical tool FEMLAB was used to implement the equations and to calculate the results. It provides a graphical user interface for the implementation and for the analysis of the results. Further on predefined application modi could be used to implement the model equations.

A suitable operating range of the solid oxide fuel cell under variation of the inlet temperature and inlet velocity of the cathode gas as well as the anode gas could be predicted. For a current density of $i_{el,avg} = 250\,mA\,cm^2$ exemplary simulation results are shown. The co-flow mode is to be preferred because of the high temperatures within the active cell area for the counter-flow mode. The operating range is determined in terms of temperature and amount of cathode air used. Further on temperature limitations are considered.

References

[1] E. Achenbach, Three-dimensional and time-dependent simulation of a planar solid oxid fuel cell stack, J. Power Sources 49 (1994) 333–348.
[2] H. Yakabe, T. Ogiwara, M. Hishinuma, I. Yasuda, 3-D model calculation for planar SOFC, J. Power Sources 102 (2001) 144–154.
[3] L. Petruzzi, S. Cocchi, F. Fineschi, A global thermo-electrochemical model for SOFC systems design and engineering, J. Power Sources 118 (2003) 96–107.
[4] P. Aguiar, D. Chadwick, L. Kershenbaum, Effect of methane slippage on a indirect internal reforming solid oxide fuel cell, Chem. Eng. Sci. 59 (2004) 87–97.
[5] P. Aguiar, C.S. Adjiman, N.P. Brandom, IT DIR-SOFC: co-flow versus counter-flow operation, in: M. Mogensen (Ed.), Sixth European Solid Oxide Fuel Cell Forum, vol. 2, Lucerne, Switzerland, 2004, pp. 617–624.
[6] P. Linstrom, W. Mallard, NIST Chemistry WebBook, NIST Standard Reference Database Number 69, http://webbook.nist.gov/chemistry, March 2003.
[7] P. Heidebrecht, K. Sundmacher, Molten carbonate fuel cell (MCFC) with internal reforming: model-based analysis of cell dynamics, Chem. Eng. Sci. 58 (2003) 1029–1036.
[8] R. Perry, D. Green, Perry's Chemical Engineers' Handbook, seventh ed., McGraw-Hill International Editions, New York, 1997.
[9] I. Drescher, Kinetik der Methan-Dampf-Reformierung, Dissertation, RWTH Aachen, 1999.
[10] FEMLAB Reference Manual, Stockholm, 2003.
[11] FEMLAB Users Guide and Introduction, Stockholm, 2003.
[12] S. Chan, K. Khor, Z. Xia, A complete polarization model of a solid oxide fuel cell and its sensitivity to the change of cell component thickness, J. Power Sources 93 (2001) 130–140.